Design and Performance Analysis of Tachyon: A Low-Altitude Hypersonic Glide Vehicle

Jackson Dendy*, Jackson Hayes†, Jacob Ramsey‡
University of Tennessee, Knoxville, Tennessee, 37996

This paper outlines the design evolution and performance of Tachyon: a highly maneuverable, low-altitude hypersonic glide vehicle designed by the Student Space Technology Association (SSTA) for the University Consortium for Applied Hypersonics' (UCAH) Undergraduate Design Competition. The design was selected as one of four nationwide winners, with praise given for its originality and performance. The competition guidelines specified a vehicle capable of unpowered flight within a velocity envelope of Mach 2-8, capable of maneuvering at up to 15 Gs, with an altitude ceiling of 9 kilometers. The design was optimized toward a high lift-to-drag ratio, thus eliciting extensive downrange performance. Furthermore, the vehicle remained stable and thermally survivable across the flight envelope. Manufacturability and cost were also key factors in the selection of the external geometry, leading to a simple double-wedge lifting-body design, aided in stability by six aft-mounted fins. These parameters coalesced into a craft with a predicted maximum lift-to-drag ratio of over 4.5. The vehicle's properties were then integrated into an in-house simulator, which was utilized for informed mission design. A trajectory was then optimized subject to constraints such as the terminal Mach, altitude ceiling, and angle of attack envelope, which yielded a downrange of 100 km.

I. Nomenclature

C_D	Drag coefficient
C_L	Lift coefficient
C_{Mx}	Rolling moment coefficient
C_{My}	Pitching moment coefficient
C_{Mz}	Yawing moment coefficient
L/D	Lift-to-drag ratio
L_{HT}	Horizontal tail moment arm, m
M_∞	Freestream Mach number
S_{HT}	Horizontal tail planform area, m^2
S_W	Wing (front lifting surface) planform area, m^2
$\bar{C}_W$	Mean fin chord, m
c_{HT}	Horizontal tail volume coefficient

*Undergraduate Student, University of Tennessee Knoxville, AIAA Student Member 1923236
†Undergraduate Student, University of Tennessee Knoxville, AIAA Student Member 1923931
‡Undergraduate Student, University of Tennessee Knoxville, AIAA Student Member 1927884

Greek Symbols

α	Angle of attack, deg
β	Sideslip angle, deg
ζ	Damping ratio
ω_n	Natural frequency, rad/s
ΔC_D	Incremental drag coefficient due to trim

Subscripts

α	Derivative w.r.t. angle of attack
β	Derivative w.r.t. sideslip
HT	Horizontal tail
W	Wing
∞	Freestream condition

II. Introduction

Hypersonic flight technology is of great interest in the modern defense landscape. Since the 1950s, hypersonics have been on the cutting edge of defense technology, with test campaigns such as the X-15 program providing many of the fundamental insights that modern hypersonic projects are based on [1]. As understanding of the hypersonic flight regime has continued to mature, the barrier of entry to developing such a vehicle has been substantially reduced. What was once relegated to some of the most secret and well-funded government projects can now be pursued at the undergraduate level. In 2025, the University Consortium for Applied Hypersonics (UCAH) hosted an Undergraduate Vehicle Design Competition where students across the country aimed to build a low-altitude, unpowered, maneuverable flight vehicle. [2] At the University of Tennessee, Knoxville, the Student Space Technology Association (SSTA) entered the competition with a group of ten undergraduate sophomores and juniors. Over 4 months, the students developed a hypersonic glide body called Tachyon. The vehicle was selected as a winner of the competition, receiving praise from premier hypersonic entities (UCAH, JHTO*) for being a thorough, original design. This paper will detail the evolution of the Tachyon external geometry, as well as the aerodynamic performance and mission plan of the final design.

III. Mission Requirements

Design constraints required Tachyon to be both cost-effective and easy to manufacture, with an emphasis placed on prioritizing additive manufacturing techniques. Furthermore, the vehicle needed to carry a cylindrical payload 0.161 m long and 0.0640 m in diameter that weighs 9 kg. Since the vehicle was constrained to a 1 m long, 0.2 m diameter cylinder, this heavily influenced the external shaping. Thermally, the vehicle needed to survive the duration of the flight without the use of ablatives while maintaining the payload and avionics below $74°C$. All of the mission constraints and requirements are outlined in Table 1.

*Joint Hypersonic Transition Office

Table 1 UCAH 2025 Undergraduate Hypersonic Flight Design Competition: Mission Requirements

Requirement	Specification
Flight regime	Mach 5–8
Stability & trim	Aerodynamically stable in all 3 axes
Objective	Maximum range and affordable manufacturability
Maximum length	1.0 m
Maximum diameter (overall)	0.2 m
Altitude Ceiling	9 km
Maneuverability	Sustain a $\geq$15 g maneuver at the 9 km ceiling altitude
Mass limits	Total mass: 45 kg; payload mass: 9.0 kg
Payload	Cylinder: 0.161 m long, 0.0640 m diameter
Thermal survivability	Survive thermal loading across flight; payload and avionics stay under $74°C$

IV. Design Evolution

The vehicle's early geometry selection was primarily driven by manufacturability. Hypersonic vehicles operate in thermally strenuous environments that require the use of exotic materials like Inconel and tungsten, which are prohibitively difficult to manufacture. Modern high lift-to-drag (L/D) hypersonic vehicles, like the X-51B[3], pursue complex waverider shaping for aerodynamic performance at the cost of manufacturability and price. The opposite design philosophy was used in this vehicle's design process, with simple wedge shaping akin to the X-43 being pursued instead of complex geometries. [4] Although the use of exotic components is unavoidable in a project such as this, a simpler shape means that these materials can be utilized more economically.

A. The Mk2 Concept

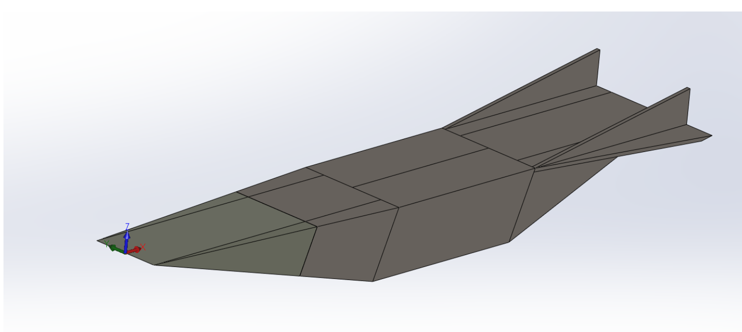

Fig. 1 Mk2: An early vehicle concept

In Fig. 1, a vehicle similar in shape to the X-43 can be seen. [4] This design featured horizontal stabilizers perpendicular to the body and a distinct wedge design. It also features a tapered tail for drag reduction. However, there were multiple concerns with this design. The vertical stabilizers were identified as a potentially large source of drag due to the shock interaction between them at high Mach numbers. [5] Later designs opted to add cant to the fins to reduce this effect. Furthermore, the small fins failed to fully utilize the allotted design space. The boat tail could also be further tapered from the sides to reduce the wake created by the vehicle, which further reduces drag. Finally, this vehicle was highly unstable in the pitch axis. Historically, vehicles take advantage of heavy tanks and engines to increase stability margin without increasing drag; however, the vehicle's unpowered nature makes this strategy impossible.

B. The Mk10 Concept

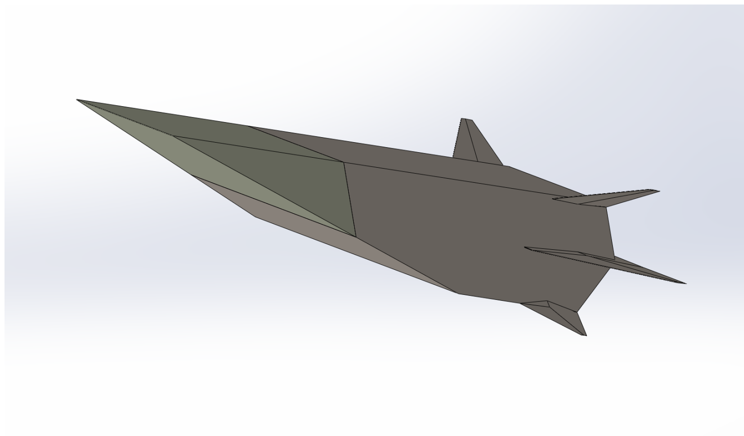

Fig. 2 Mk10: A preliminary vehicle concept

Figure 2 is another initial concept of Tachyon that addresses some of the shortcomings of the previous iteration. First, the vertical stabilizers and boat tail were canted and tapered to reduce the drag on the vehicle. This concept still features a wedge design but demonstrated more efficient utilization of space with another set of fins placed at the bottom of the vehicle, creating a six fin arrangement. The low-fidelity analysis of this concept demonstrated a maximum L/D of 7; however, it was still highly unstable in the pitch axis. To resolve this problem, two plans were jointly executed: one was maximizing fin efficacy, and the other was the fore placement of a tungsten counterweight.

C. Final Design

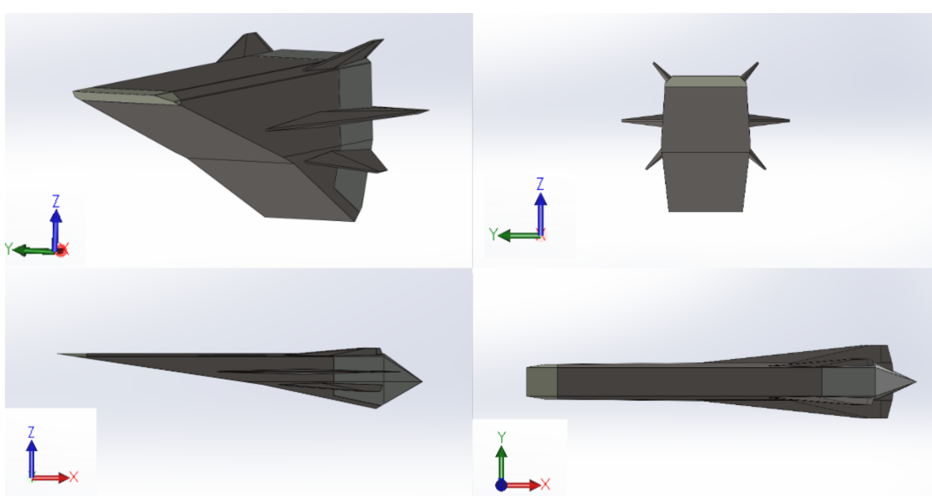

Fig. 3 Tachyon: Final design

Figure 3 displays the final external geometry selected for Tachyon. The design features an unusual double wedge design. The aft wedge was positioned to produce a large lift vector behind the center of mass, thus increasing stability margin. Furthermore, the fillet on the front of the vehicle was adjusted to machine tolerance instead of a point edge. The aft of the body features a similar six-fin arrangement with a tapered boat tail. The top set of fins is canted to reduce the amount of drag created by the shock interactions between the vertical stabilizers. The root chords of the fins were drastically increased to maximize the space made available by the geometry constraints. The wings have a sweep angle of 80° and a larger fillet than the nose to sustain the thermal loads imparted on the Inconel X-750 leading edges during flight. Inside the Inconel 718 skin lies a tungsten counterweight for stability purposes. The counterweight also acts as a heat sink to pull heat away from the payload bay located in the middle of the vehicle.

1. Vehicle Sizing

Within the geometric constraints, the final configuration was sized to meet aerodynamic, trim, and heating requirements. As mentioned above, the majority of the lift is produced on the front of the vehicle; thus, a large tail is needed to counter the nose-up moment. The sizing of the horizontal tail is given by [6]:

$$S_{HT} = \frac{c_{HT}\bar{C}_W S_W}{L_{HT}}$$

Where c_{HT} is the horizontal tail volume coefficient and is taken to be 0.8 as a first approximation, $\bar{C}_W$ is the mean tail chord, S_W is the tail lifting area, and L_{HT} is the horizontal moment arm of the tail. Since the moment being countered is that of the frontal section of the fuselage, the tail properties are taken to be those of the frontal underside area. With $S_W = 0.0521\,\text{m}^2$, $\bar{C}_W = 0.550\,\text{m}$, and $L_{HT} = 0.300\,\text{m}$, a desired tail area of $0.0763\,\text{m}^2$ is calculated. The total area of the back underside lifting surface and planform area of the fins is $0.0674\,\text{m}^2$, which is 15% smaller than desired due to conflicting considerations for the tail sizing.

Although all aerodynamics requirements are met, the final sizing is dominated by thermal considerations. The fins are made thermally survivable with blunted leading edges and large sweep angles, at the expense of stability and aerodynamic performance. The planform areas of the top fin, mid fin, and bottom fin are $0.00361\,\text{m}^2$, $0.0114\,\text{m}^2$, and $0.00354\,\text{m}^2$ respectively. The planform areas of the mid and top fin control surfaces are $0.000954\,\text{m}^2$ and $0.000307\,\text{m}^2$.

V. Aerodynamic Performance

The aerodynamic performance of Tachyon was assessed using a combination of industry-grade software and in-house simulations. For preliminary analysis, NASA's Configuration Based Aerodynamics (CBAERO) [7], a panel method code, was used to rapidly assess and iterate on early designs. CBAERO is computationally inexpensive relative to Computational Fluid Dynamics (CFD), allowing for aerodynamic databases to be generated in minutes for early designs. Since Tachyon was designed across a 4 month time frame, CBAERO was crucial to making informed decisions toward a final design. After a final design was established, NASA's FUN3D [8] CFD code was used to characterize the performance of the vehicle; specifically, an aerodynamic database was created across the flight envelope of Mach 2-8 and -5° to 5° angle of attack. While static stability was derived from moment data, the competition also required the analysis of longitudinal dynamic stability. Thus, an aircraft pitch dynamics simulation was created by the Tachyon team.

A. Aerodynamics Characteristics

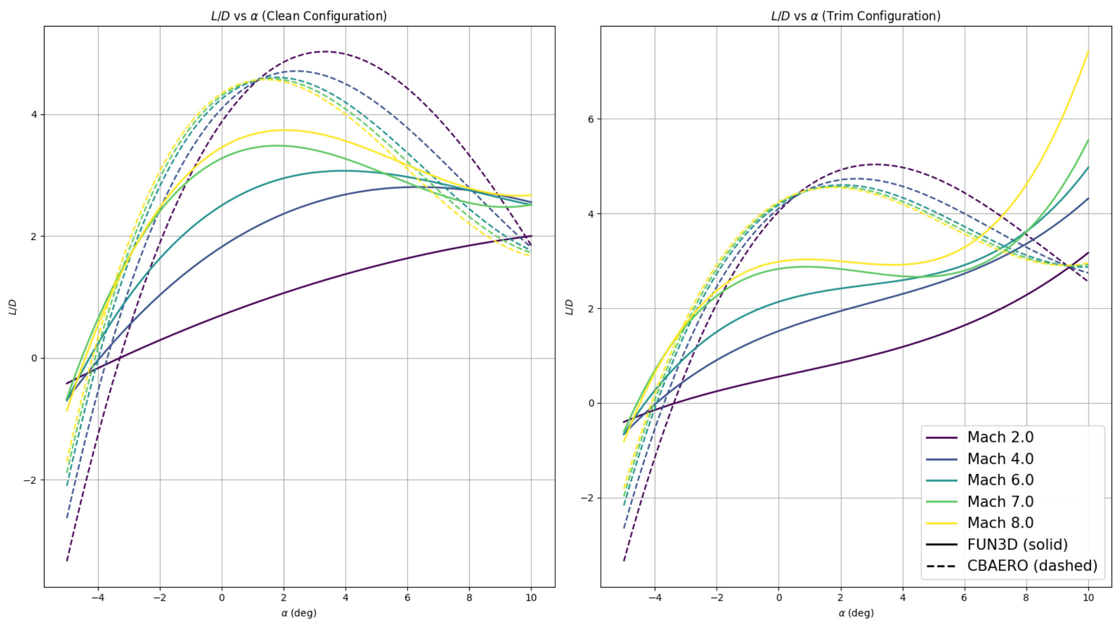

Fig. 4 This plot displays the aerodynamic performance of Tachyon evaluated by CBAERO and FUN3D in the trimmed and clean configuration.

Aerodynamic performance was assessed through the aerodynamic database created in FUN3D and CBAERO. Displayed in Fig. 4 is the L/D from both tools over the expected flight envelope, covering a range of α and M_∞ values. The trimmed condition is defined as the configuration of the vehicle in which constant control surface deflections are utilized to maintain favorable stability characteristics. Both the clean and trim configurations are shown for comparison. The L/D curve in CBAERO is, as expected, a parabolic curve. However, additional 3D effects become evident from the FUN3D results. For both the trimmed and clean configurations, CBAERO consistently over-predicts L/D compared to FUN3D. For the trimmed configuration, the L/D spikes at high α, which is likely unrealistic. The maximum L/D value near the nominal cruise condition was found to be 4.79 in CBAERO for the clean configuration, whereas it was only 3.67 in FUN3D. These values are in sufficiently good agreement in the α regions of interest.

1. Longitudinal Stability

The pitching moment derivative with respect to angle of attack, C_{My_α}, is obtained through a linear least squares regression of data points output by CBAERO and FUN3D seen in Fig. 5. Dynamic pitch stability is demonstrated in Fig. 6 via a root locus diagram with operating points taken at Mach 2, 4, 6, 7, 8 with a zero pitch angle, pitch rate, and vertical velocity.

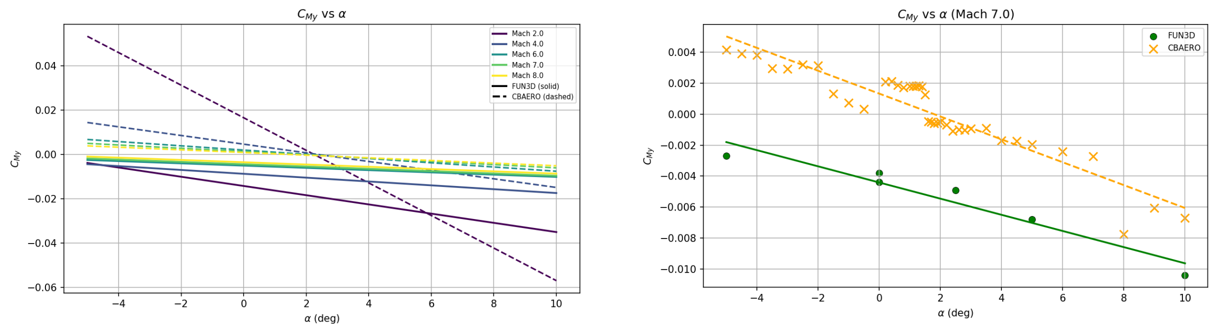

(a) Pitching moment vs. α for full Mach range

(b) Pitching moment curve at Mach 7

Fig. 5 Pitching moment characteristics across Mach range and at Mach 7 with zero sideslip

As calculated from CFD results at Mach 7, Tachyon has a positive static margin of 12.73% in pitch. However, the vehicle has unfavorable trim characteristics in a clean configuration, as the entire moment curve is nose-down from CFD. Thus, a deflection of 2.5° to the elevators was modeled in CBAERO to approximate the drag incurred by a trimmed configuration. The change in C_d from trim deflection, ΔC_D, was extracted from the subtraction of clean and trim CBAERO drag. This was then added to the CFD results to generate Fig. 4. The L/D peak decreased to 3.00 with the addition of trim drag.

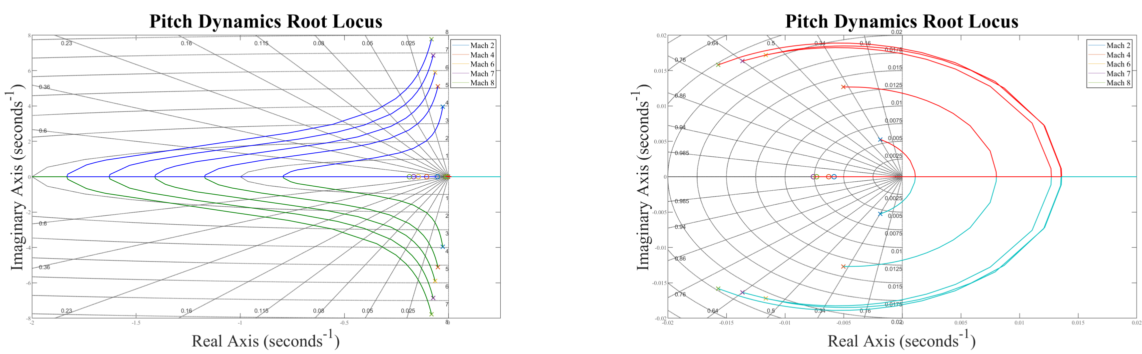

(a) Short period mode

(b) Phugoid mode

Fig. 6 Root Locus of Tachyon's longitudinal dynamics at selected Mach numbers

Figure 5a clearly demonstrates static stability along the longitudinal axis as the $\frac{\partial C_{M_y}}{\partial \alpha}$ is negative. [9] Figure 6a displays the stability of the short period mode with poles denoted x lying in the left half plane. The damping ratio ζ and natural frequency were found to be $\zeta = 0.07 - 0.0105$ and $\omega_n = 3.95 - 7.77\,\mathrm{s}^{-1}$. Figure 6b demonstrates stability of the phugoid mode for the same reasons with $\zeta = 0.334 - 0.704$ and $\omega_n = 0.0056 - 0.223\,\mathrm{s}^{-1}$.

2. Lateral and Directional Stability

To assess yaw and roll stability, sideslip cases at $\alpha = 0°$ are run in FUN3D and CBAERO. Stability is demonstrated through a negative yawing and rolling moment derivative with respect to sideslip, C_{Mx_β} and C_{Mz_β}, seen in Fig. 7. [10]

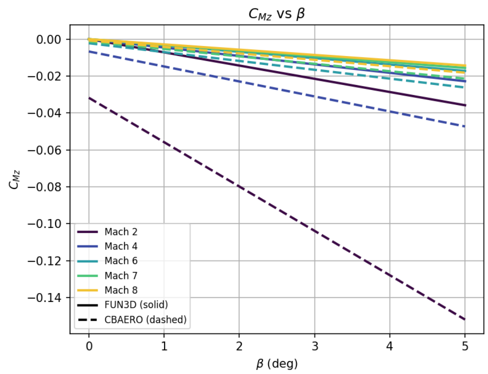

(a) Yawing moment vs β

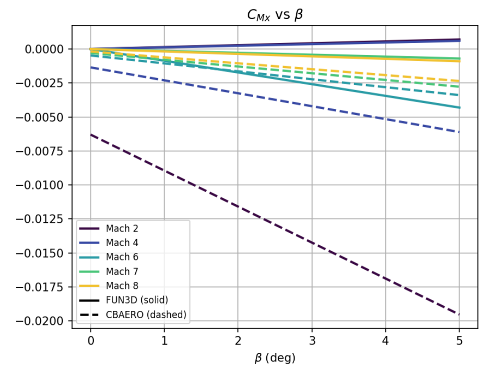

(b) Rolling moment vs β

Fig. 7 Yawing and rolling moments vs β across Mach range

While yaw stability is achieved throughout the entire range of Mach numbers, the vehicle is unstable in roll without trim at Mach 2. This can be accounted for with a constant control surface deflection of the ailerons, inducing a restoring rolling moment. The additional drag incurred by the deflection of control surfaces is accounted for in trajectory analysis as explained earlier.

VI. Mission Design

A. Trajectory Generation

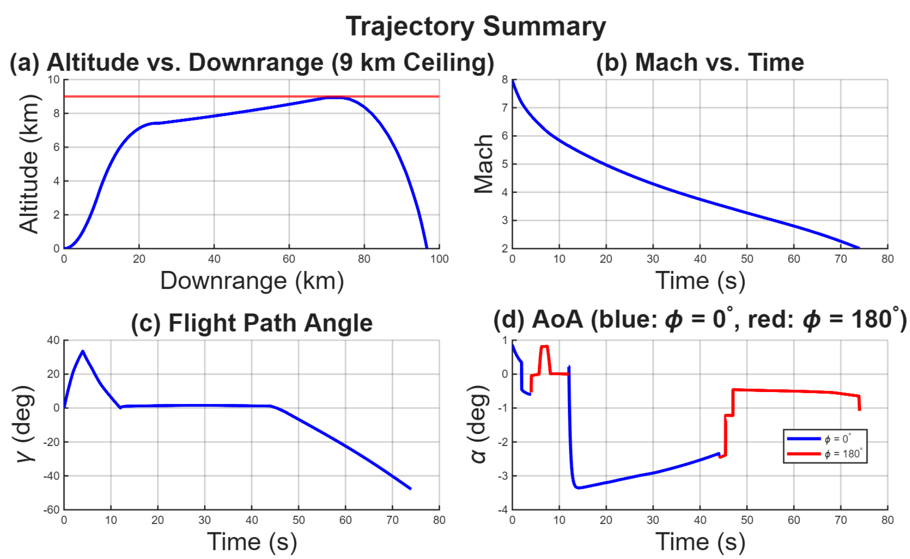

Fig. 8 Trajectory States: a) altitude plotted against downrange distance, b) Mach number plotted against time, c) flight path angle relative to the local horizontal plotted against time, d) angle of attack plotted against time.

The optimal trajectory in Fig. 8 is generated by an in-house direct solver utilizing dynamics from Grant and Braun [11]. The trajectory generation was broken into ascent and glide/dive phases. This distinction is made to make the convergence of a solution easier. The solution is found using a bounded Broyden–Fletcher–Goldfarb–Shanno minimizer [12]. The control input α needed to be bounded due to physical constraints. Based on CFD results and suspected flow separation, the input is bounded from $-7°$ to $8°$. In each phase of flight, a similar alternating schema of penalty parameter continuation and successive constraint tightening is used to ensure convergence of a solution.

1. Ascent Phase

The ascent phase began as a one-parameter optimization with the vehicle flip time acting as the input; the flip time is the time at which the vehicle rolls over 180°. The flip time is iterated on until a satisfactory altitude and flight path angle are achieved. That input profile is used as an initial guess for the optimization solution, which aimed for a cruise altitude of 7.5 km. The terminal constraints are applied successively in the order of altitude, flight path angle, and velocity. The final terminal constraint applies a negated squared terminal velocity to maximize the final velocity for glide. After a satisfactory final condition for ascent is reached, that solution is used as an initial state for the glide phase. The flip time for Tachyon's trajectory was found to be 4 s.

2. Glide and Dive Phase

The glide phase also has a flip time to begin diving toward the ground; however, the initial guess also must have a varying angle of attack. To solve this problem, a temporary feedback controller to regulate the vertical velocity was introduced until dive, where α is held constant. The dive α is iterated until the vehicle's terminal altitude is close to 0. In a similar fashion to the ascent phase, the initial input guess is given to the optimizer for further refinement. First, the altitude constraint is applied at the ground. Next, the final velocity is constrained to Mach 2. This step frequently sees the solution jump above the altitude ceiling. Two paths are explored to find a permissible solution to this problem. The first is to apply a soft path constraint for exceeding 9 km of altitude; however, this causes over 10x longer run times and proves ineffective for significant violations of the constraint. The second path is to iterate on an ascent profile until one is found that results in a permissible glide profile. Ultimately, the latter option was selected. The final term in the cost function is a maximization of the downrange angle. The final conditions for this optimal trajectory are as follows: downrange = 96.7 km, $M_\infty = 2$. The altitude constraint is also satisfied with an impact at sea level and a ceiling of 8.9 km.

B. Launch Apparatus

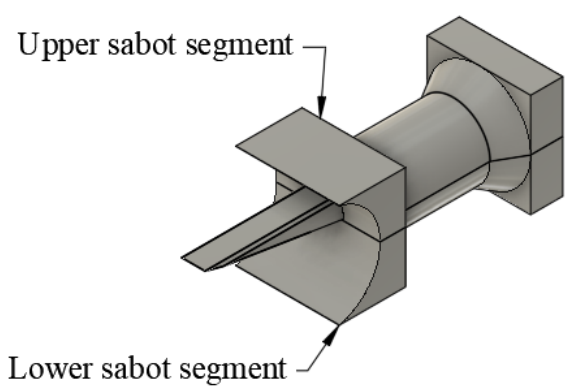

Fig. 9 Tachyon within the Sabot

The launch system selected for Tachyon is an electromagnetic rail gun. This system requires Tachyon to be enclosed within a sabot, with symmetric sabot separation being essential for a stable post-launch vehicle acceleration profile. During launch, two phases of shock wave interactions can be observed:

1) The interaction between the projectile and the shock waves induced by the rail gun acceleration
2) The interaction between the projectile and the sabot after muzzle-exit through the shock waves

Based on the research by Yang et al [13], α should be constrained to [-2, 2] to eliminate unstable 2nd phase shock wave interactions. The conceptual design for Tachyon's surrounding sabot can be seen in Fig. 9. A dual pedal sabot was designed to protect and support Tachyon throughout launch and prevent bore balloting.

VII. Conclusion

To satisfy the stringent requirements outlined by UCAH's Undergraduate Design Competition, the University of Tennessee's SSTA designed Tachyon: a vehicle capable of sustained, unpowered hypersonic flight below a 9 km altitude ceiling, culminating in a Mach 2 impact nearly 100 km downrange. Tachyon's robust design also enables the vehicle to sustain a turn of well over 15 g. Throughout the flight envelope, Tachyon exhibits favorable stability characteristics in all phases of flight, with the only exception occurring in the roll axis at low Mach; however, this can be corrected with proper trim. All of these attributes, combined with the simplicity of the design, directly contributed to the vehicle being chosen as the overall winner of the UCAH competition.

References

[1] NASA, "X-15: Hypersonic Research Program," `https://www.nasa.gov/reference/x-15/`, 2026. Accessed: 10-Feb-2026.

[2] Texas A&M University Hypersonics Laboratory, "2025 Undergraduate Hypersonic Flight Design Competition," `https://hypersonics.tamu.edu/2025-undergraduate-hypersonic-flight-design-competition/`, 2025. Accessed: 10-Feb-2026.

[3] Lane, J., "Design Processes and Criteria for the X-51A Flight Vehicle Airframe," *UAV Design Processes / Design Criteria for Structures — RTO-MP-AVT-145*, NATO RTO, 2007, pp. 1.7–1–1.7–14. Presented at UAV Design Processes / Design Criteria for Structures, Neuilly-sur-Seine, France.

[4] Marshall, L. A., Bahm, C., Corpening, G. P., and Sherrill, R., "Overview With Results and Lessons Learned of the X-43A Mach 10 Flight," *AIAA/CIRA 13th International Space Planes and Hypersonic Systems and Technologies Conference*, 2005. URL `https://ntrs.nasa.gov/api/citations/20050175679/downloads/20050175679.pdf`, document ID 20050175679.

[5] Anderson, J. D., *Hypersonic and High Temperature Gas Dynamics*, 2nd ed., American Institute of Aeronautics and Astronautics, Reston, VA, 2006.

[6] Raymer, D. P., *Aircraft Design: A Conceptual Approach*, 7th ed., American Institute of Aeronautics and Astronautics, Reston, VA, 2021.

[7] "Configuration-Based Aerodynamics (CBAero) (ARC-15819-1)," `https://software.nasa.gov/software/ARC-15819-1`, 2025.

[8] *FUN3D Manual*, 2025. URL `\url{https://fun3d.larc.nasa.gov/}`, accessed: 2025-11-11.

[9] Anderson, J. D., *Aircraft Performance and Design*, McGraw–Hill, New York, 1999.

[10] Raymer, D. P., *Aircraft Design: A Conceptual Approach*, 7th ed., American Institute of Aeronautics and Astronautics, Reston, VA, 2021.

[11] Grant, M. J., and Braun, R. D., "Rapid Indirect Trajectory Optimization for Conceptual Design of Hypersonic Missions," *AIAA Guidance, Navigation, and Control Conference*, American Institute of Aeronautics and Astronautics, Toronto, Ontario, Canada, 2010. https://doi.org/10.2514/1.A32949.

[12] Zhu, C., Byrd, R. H., Lu, P., and Nocedal, J., "Algorithm 778: L-BFGS-B: Fortran Subroutines for Large-Scale Bound-Constrained Optimization," *ACM Transactions on Mathematical Software*, Vol. 23, No. 4, 1997, pp. 550–560. https://doi.org/10.1145/279232.279236.

[13] Xuefeng Yang, B. L. S. T., Junyong Lu, and Xie, Z., "Three-Dimensional Numerical Investigation of the Asymmetric Discard Characteristics of Hypervelocity Projectile Sabot," *Aerospace*, 2025.